

Supplementary Information for

Enhanced Stability and Optical Performance of $\text{CsPbBr}_3@\text{FAPbBr}_3$ Core–Shell Perovskite Nanocrystals

Danila A. Tatarinov, Azat O. Ismagilov, Aleksandra V. Koroleva, Evgeniy V. Zhizhin, Weitao Zheng, Aleksander V. Baranov, and Aleksandr P. Litvin*

E-mail: litvin@jlu.edu.cn

Perovskite NC Molar Concentration and Multiphoton Absorption Cross-Section Calculations

These calculations were adapted from a previous reported procedure.¹ The perovskite NC extinction coefficient (ε) at 400 nm was calculated from the following equation:

$$0\mu = \frac{D}{C_M l} = \frac{m_{NC} D}{C_{mass} l} = \frac{N_A B \epsilon^{\text{TM}} V_{NC} B \epsilon^{\text{TM}} \Pi \Gamma D}{C_{mass} l}, \quad (\text{S1})$$

where D is the absorbance of the sample at 400 nm; C_M is NC molar concentration; l is cuvette length; m_{NC} is molar mass of the single NC; C_{mass} is mass concentration; N_A is the Avogadro number; V_{NC} is NC volume (determined from the NC size); ρ is the NC density. NC density was calculated by normalizing the crystalline cell mass to the cell volume:

$$\Pi \Gamma = \frac{m_{cell}}{V_{cell}} = \frac{m_{cell}}{r^3}, \quad (\text{S2})$$

where m_{cell} and V_{cell} are the respective cell mass and cell volume, r is the edge length, determined from TEM (see Figure 1c,d). Cell mass was calculated from known NC stoichiometry. Mass concentration of the solution was determined from the weight of thoroughly washed and dried NCs.

Concentrations of NCs and Rhodamine 6G were determined from Beer's law. For Rhodamine 6G, the known extinction coefficient ($\sim 40,000 \text{ mol}^{-1}\text{cm}^{-1}$) at 500 nm was used.^{2,3}

Rhodamine 6G in ethanol was used as a standard for calculating the 2PA cross section. The cross section of Rhodamine 6G was taken to be $128 \pm 84 \text{ GM}$ ($10^{-50} \cdot \text{cm}^4 \cdot \text{s} \cdot \text{photon}^{-1}$), as averaged from the literature data (obtained at 800 nm with a pulse duration of 100 fs).^{4–6} To estimate the 2PA cross section, the PL was first measured under single-photon excitation. The PL was measured relative to the standard rhodamine 6G in ethanol (PL ~ 0.9). The PL quantum yield was calculated using equation S3:

$$\Pi \dagger_s = \Pi \dagger_r \frac{I_s D_r}{I_r D_s} \left(\frac{n_r}{n_s} \right)^2, \quad (\text{S3})$$

where φ is the PL quantum yield under one-photon excitation; I is the area of the PL spectra, D is the optical density at the excitation wavelength, n is the refractive index of the solution; the indices r and s represent the values for the referent standard and sample, respectively.

Then the 2PA cross section was calculated using equation S4:

$$\Pi \dot{\Gamma}_s^{2PA} O_s = \Pi \dot{\Gamma}_r^{2PA} O_r \frac{\Pi \dagger_r I_s^{2P} C_r n_r}{\Pi \dagger_s I_r^{2P} C_s n_s}, \quad (\text{S4})$$

where σ^{2PA} is the 2PA cross section (in GM); φ is the one-photon excited PL; η is the two-photon excited PL; I^{2P} is the area of the two-photon excited PL spectra, C is the concentration (in M), n is the refractive index of the solution; the indices r and s represent the values for the referent standard and sample, respectively. Provided that $\varphi = \eta$ the equation can be rewritten as follows:

$$\Pi \dot{\Gamma}_s^{2PA} = \Pi \dot{\Gamma}_r^{2PA} \frac{\Pi \dagger_r I_s^{2P} C_r n_r}{\Pi \dagger_s I_r^{2P} C_s n_s}, \quad (\text{S5})$$

Supplementary Figures

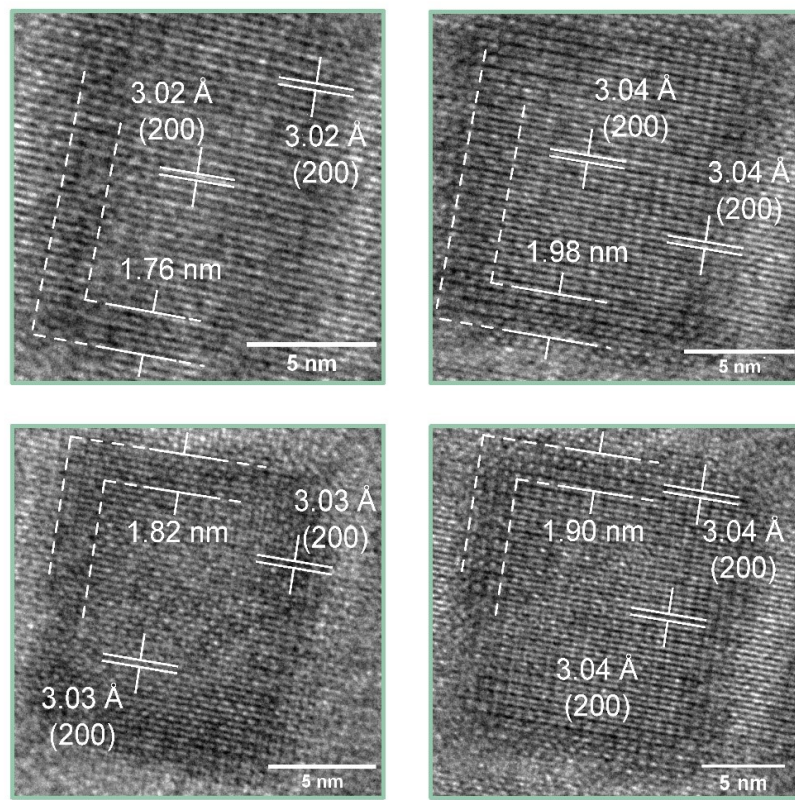


Figure S1. HR-TEM images TEM images of $\text{CsPbBr}_3@\text{FAPbBr}_3$ with estimated interplanar distances and FAPbBr_3 shell thickness.

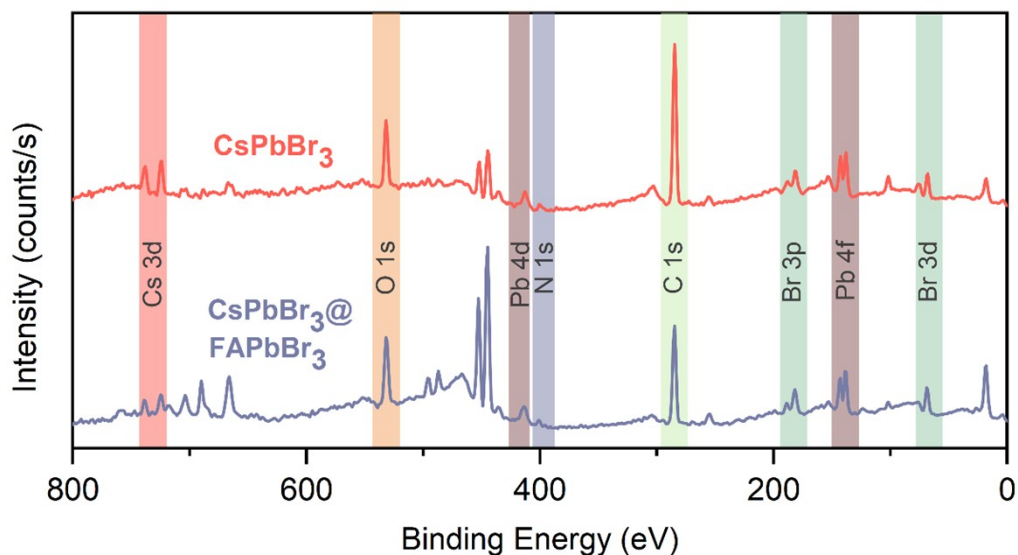


Figure S2. Survey XPS spectra for the CsPbBr_3 core (red) and $\text{CsPbBr}_3@\text{FAPbBr}_3$ core-shell (blue) NCs.

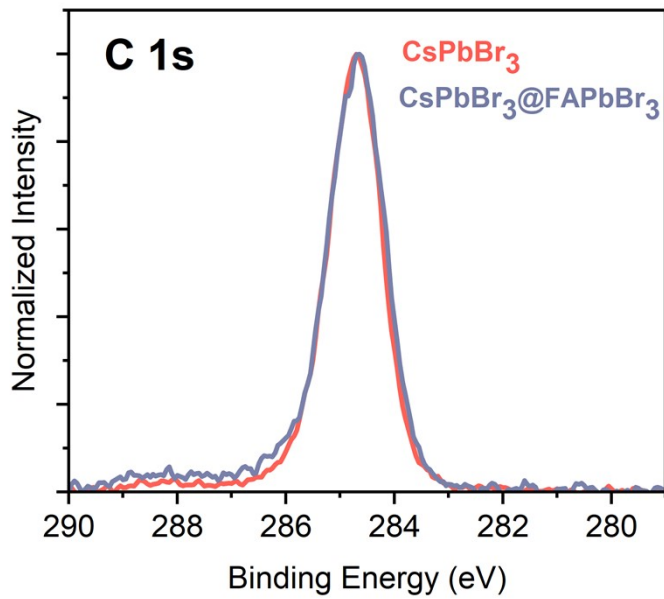


Figure S3. XPS C 1s spectra of CsPbBr_3 core (red) and $\text{CsPbBr}_3@\text{FAPbBr}_3$ core-shell (blue) NCs after the peak calibration.

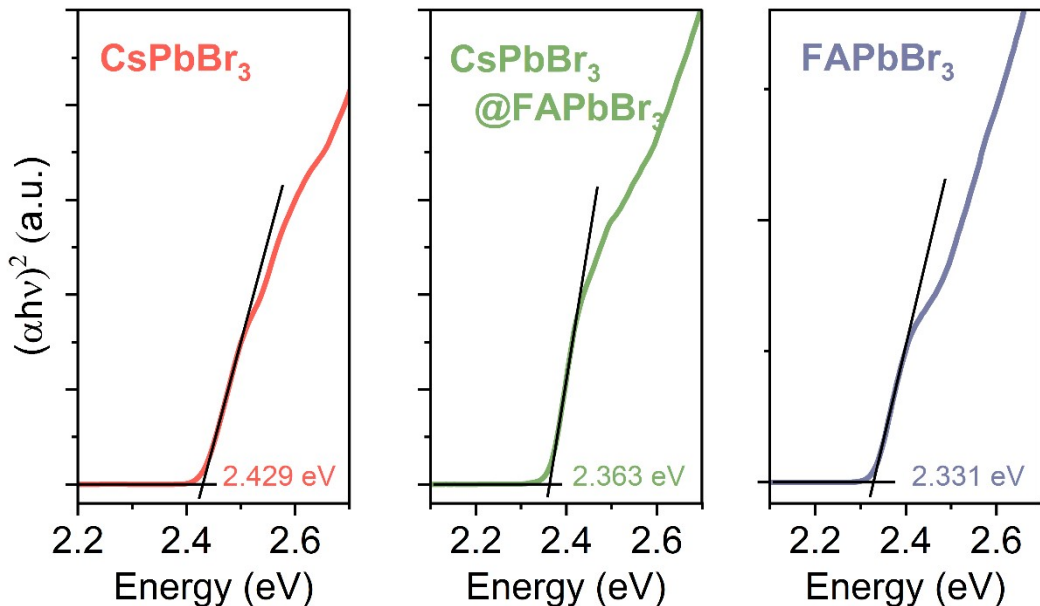


Figure S4. Tauc plots for the CsPbBr_3 core (red), $\text{CsPbBr}_3@\text{FAPbBr}_3$ core-shell (green), FAPbBr_3 (blue) NCs. The bandgaps were determined by finding the point where the linear fit of the slope intersects with the zero line.

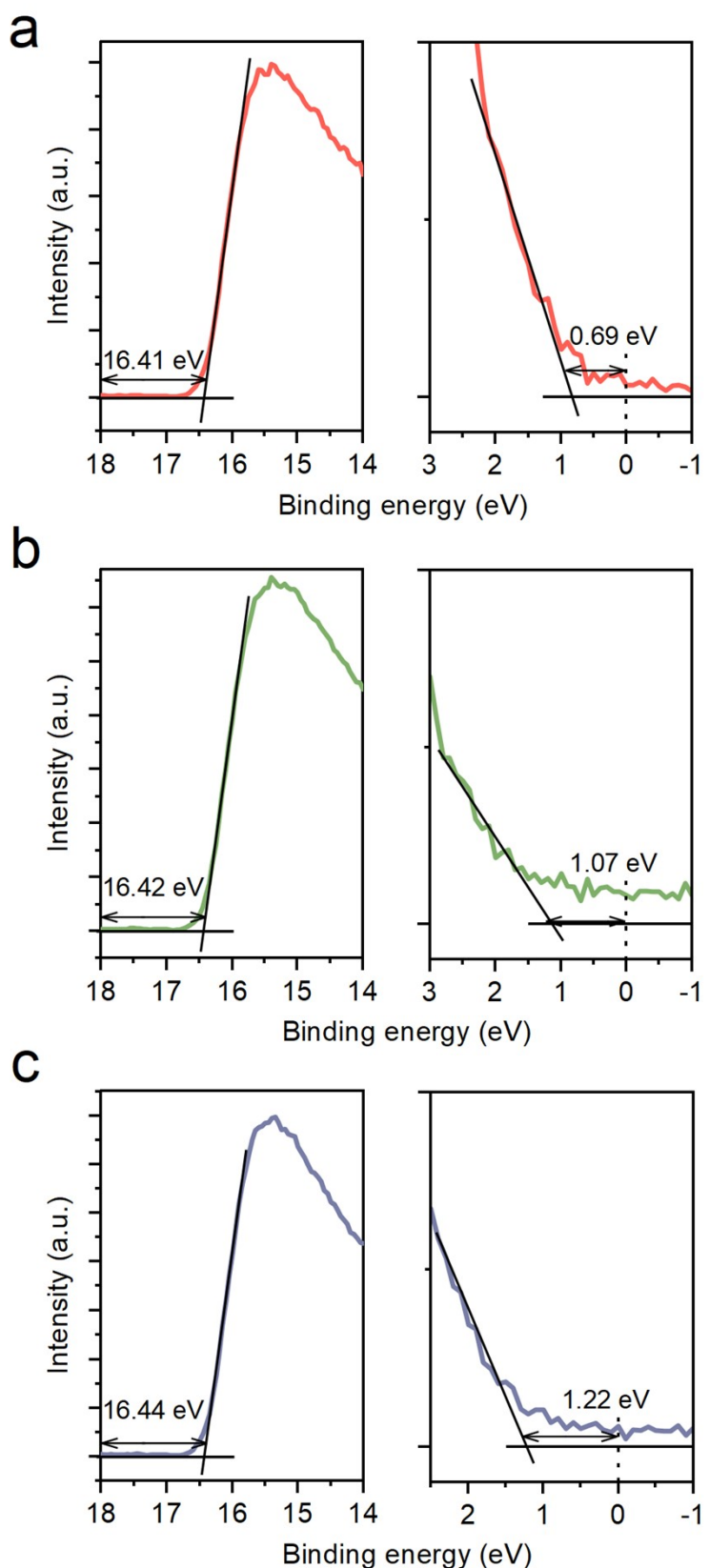


Figure S5. UPS spectra for the cutoff (left) and valence (right) regions for (a) CsPbBr_3 core, (b) $\text{CsPbBr}_3@\text{FAPbBr}_3$ core-shell, (c) FAPbBr_3 NCs.

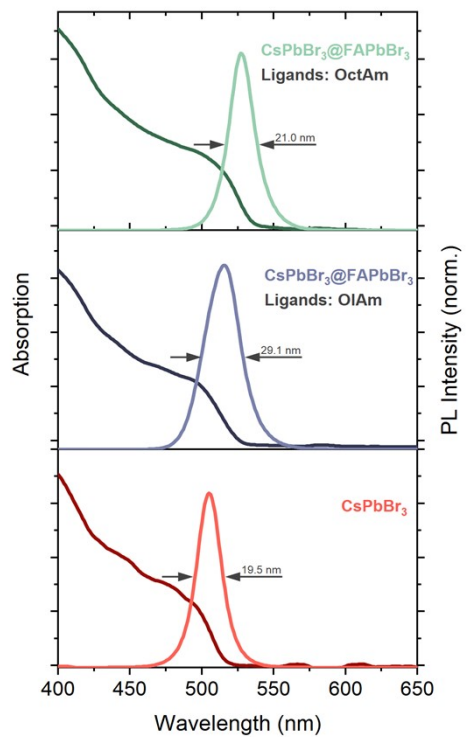


Figure S6. Absorption and PL spectra of CsPbBr_3 core (red) and $\text{CsPbBr}_3@F\text{APbBr}_3$ core-shell NCs synthesized with oleylamine (blue) and octylamine (green).

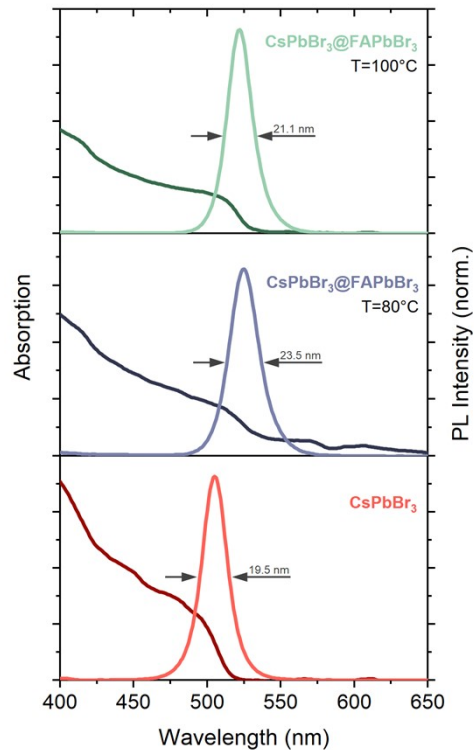


Figure S7. Absorption and PL spectra of CsPbBr_3 core (red) and $\text{CsPbBr}_3@F\text{APbBr}_3$ core-shell NCs synthesized with oleylamine (blue) and octylamine (green).

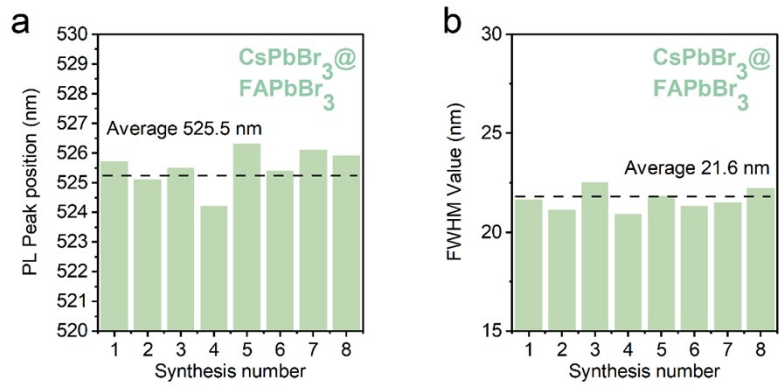


Figure S8. Reproducibility of (a) PL Peak position and (b) PL FWHM of $\text{CsPbBr}_3@\text{FAPbBr}_3$ core-shell NCs synthesized with octylamine.

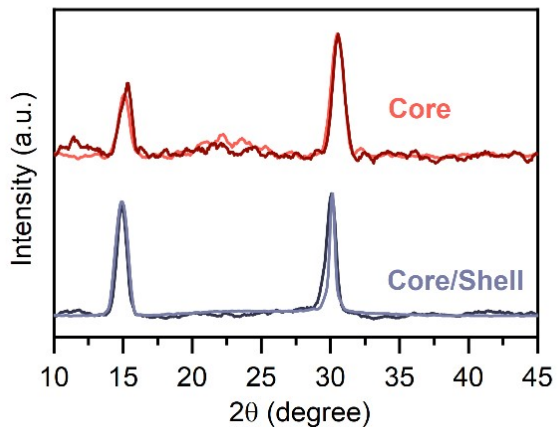


Figure S9. Comparison of XRD patterns obtained for the CsPbBr_3 (red) and $\text{CsPbBr}_3@\text{FAPbBr}_3$ (blue) NCs after being stored for 2 months.

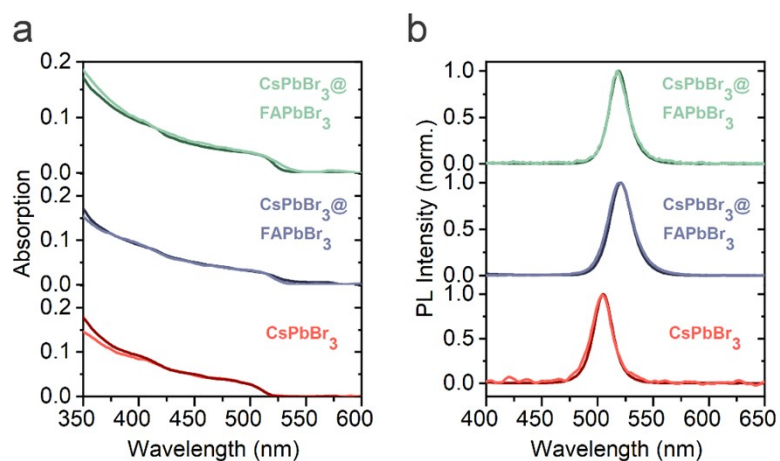


Figure S10. Comparison of absorption (a) and PL (b) spectra of CsPbBr_3 core (red) and $\text{CsPbBr}_3@\text{FAPbBr}_3$ core-shell NCs synthesized at 80°C (blue) and 100°C (green) after being stored for 2 months.

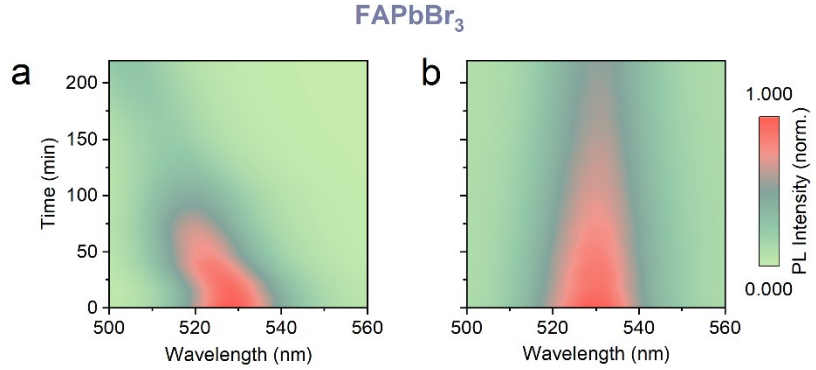


Figure S11. The photo- (a) and thermostability (b) of the PL spectra for FAPbBr₃ NCs.

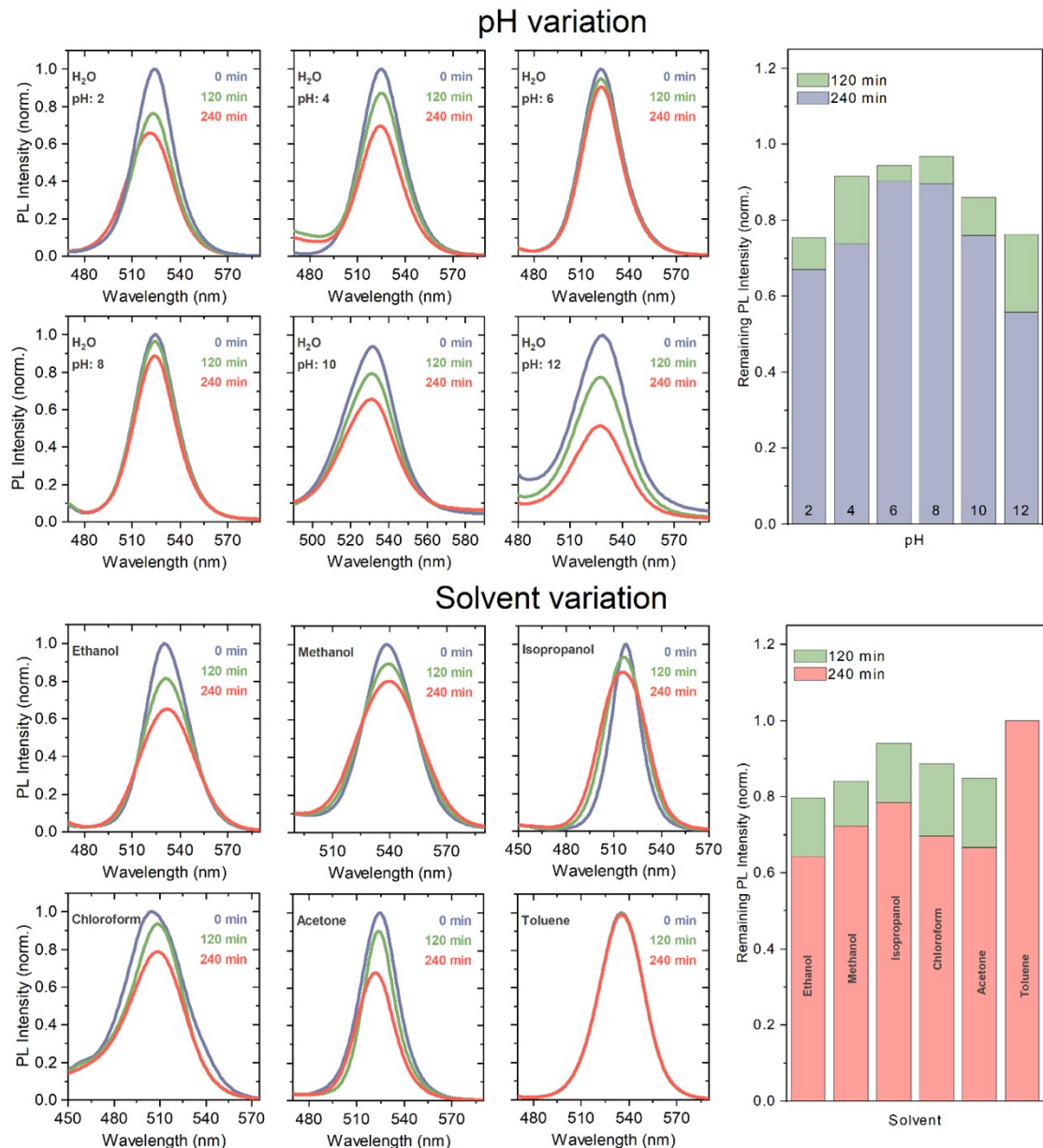


Figure S12. Comparison of the stability for the SiO₂-coated CsPbBr₃@FAPbBr₃ core-shell NCs at various pH values (upper panel) and in various solvents (bottom panel). The bar graphs represent the remaining PL intensity after 120 and 240 min in the corresponding solvents.

Supplementary Tables

Table S1. The results of the fitting of PL decay curves recorded for CsPbBr₃ core and CsPbBr₃@FAPbBr₃ core-shell NCs.

Sample	Intensity-averaged PL lifetime, ns	A ₁ (kCnts)	τ ₁ , ns	A ₂ (kCnts)	τ ₂ , ns	A ₃ (kCnts)	τ ₃ , ns
CsPbBr ₃	13.1 ± 0.5	0.824 ± 0.004	1.68 ± 0.06	0.013 ± 0.002	49.00 ± 3.71	0.164 ± 0.002	6.51 ± 0.23
CsPbBr ₃ @FAPbBr ₃	20.5 ± 0.3	0.819 ± 0.008	9.00 ± 0.19	0.181 ± 0.008	35.00 ± 0.67	0	0
FAPbBr ₃	17.4 ± 0.3	0.434 ± 0.005	12.00 ± 0.24	0.013 ± 0.001	71.00 ± 4.31	0.552 ± 0.009	3.6 ± 0.13

Table S2. Reported values of 2PA cross-section ($\sigma^{2\text{PA}}$) for CsPbBr₃ nanocrystals (NCs), nanoplatelets (NPs), nanorods (NRs), and nanowires (NWs).

Sample	Size (nm)	$\sigma^{2\text{PA}}$ (GM)	Volume Normalized $\sigma^{2\text{PA}}$ GM×nm ⁻³)	Technique (pulse duration, repetition rate, ex. wavelength)	Ref.
CsPbBr ₃ NCs	20	3.68×10 ⁴	4.6	2PPL (100 fs, 1 kHz, 800 nm)	⁷
CsPbBr ₃ NCs	25	8.5×10 ⁴	5.44	Z-scan (100 fs, 80 MHz, 800 nm)	⁸
CsPbBr ₃ NCs	7.3	1.2×10 ⁵	308	Z-scan (100 fs, 1 kHz, 720-1200 nm)	⁹
CsPbBr ₃ NCs	20	1.4×10 ⁵	17.5	Z-scan (— fs, 1 kHz, 790-925 nm)	¹⁰
CsPbBr ₃ QDs	7	1.8×10 ⁵	525	Z-scan (100 fs, 1 kHz, 700-1500 nm)	¹¹
CsPbBr ₃ NRs	200×10	2.1×10 ⁵	105	Z-scan (100 fs, 80 MHz, 800 nm)	⁸
CsPbBr ₃ QDs	12.4	2.2×10 ⁵	115	Z-scan (— fs, 1 kHz, 800 nm)	¹²
CsPbBr ₃ NPs	10.4×7.8×1.8	2.28×10 ⁵	1562	Z-scan (100 fs, 1 kHz, 720-1200 nm)	⁹
CsPbBr ₃ NCs	12.4	(3.2±1.9)×10 ⁵	171±112	2PPL (30 fs, 800-1300 nm)	¹

CsPbBr ₃ NPs	20×4×20	4.9×10 ⁵	306	Z-scan (100 fs, 80 MHz, 800 nm)	⁸
CsPbBr ₃ NCs	12	9.8×10 ⁵	567	Z-scan (70 fs, 1 kHz, 800 nm)	¹³
CsPbBr ₃ NCs	9	1.0±0.2×10 ⁶	1372±274	Z-scan (50 fs, 1 kHz, 675-1000 nm)	¹⁴
CsPbBr ₃ NRs	61.3*11.6	1.5×10 ⁶	221	Z-scan (100 fs, 1 kHz, 800-1300 nm)	¹⁵
CsPbBr ₃ NCs	9	2.7×10 ⁶	3704	Z-scan (90 fs, 1 kHz, 800 nm)	¹⁶
CsPbBr ₃ NCs	8.3	2.7×10 ⁵	472	2PPL (30 fs, 800-1300 nm)	This work
CsPbBr ₃ @FAPbBr ₃ NCs	11.2	1.3×10 ⁶	996	2PPL (30 fs, 800-1300 nm)	This work

Table S3. Comparison of stability in water for perovskite-based composite materials, according to literature data.

Materials	Synthesis method	PL peak position	PL QY (non-polar solvent)	Size	PL stability	Application	Year	Ref.
CsPbI ₃ @ 3IS @SiO ₂ phospholipid micelles	Two-step passivation with 3IS	680 nm	91%	16 nm	45% after 6h (H ₂ O)	Bio-Imaging	2022	¹⁷
CsPbBr ₃ -SiO ₂ composites	Two-step hydrolysis of PH-TMOS	521 nm	65%	13 nm	62% PL retention after 30 min (hexane/ethanol mixture)	N/A	2021	¹⁸
CsPbBr ₃ /mSiO ₂ composites	LARP	510 nm	90%	10 nm	50% after 35 days (H ₂ O)	LEDs	2020	¹⁹
CsPbBr ₃ /mSiO ₂ nanocomposites	<i>in situ</i> template-assisted synthesis	514 nm	63%	150 nm	100% after 50 days (H ₂ O)	Biosensing	2024	²⁰
CsPbBr ₃ -SiO ₂ composites	One-step <i>in-situ</i> synthesis and encapsulation method	520 nm	84.7%	Thin films with 34.7 nm crystals	>60% for 1100 h (H ₂ O)	N/A	2023	²¹

CsPbBr ₃ /SiO ₂ nanocrystals	RT synthesis and SiO ₂ encapsulation	520 nm	N/A	140 nm	98.3% after 168 h (H ₂ O)	PL sensing	2022	²²
CsPbBr ₃ QDs/MSs	High temperature solid phase melting method	520 nm	N/A	500 nm	80% for 2 weeks (H ₂ O)	WLEDs	2022	²³
CsPbBr ₃ /SiO ₂ composites	Molten salts synthesis approach	520 nm	89 ± 10%	0.6 μm	95% after 30 days (H ₂ O)	WLEDs	2021	²⁴
DDAB-CsPbBr ₃ /SiO ₂ QDs composites	Silica-coating at room temperature	520 nm	80%	N/A	50% after 210 min (H ₂ O)	WLEDs	2021	²⁵
CsPbBr ₃ /polymer microspheres	Encapsulation in microspheres	520 nm	N/A	285 nm	100% after 28 days (H ₂ O)	Detectors	2021	²⁶
CsPbBr ₃ -SiO ₂ powders	Encapsulating derived from molecular sieve templates at high temperature	520 nm	63%	Pore size 3.6 nm length N/A	100% after 50 days (H ₂ O)	LEDs	2020	²⁷
CsPbBr ₃ /mSiO ₂ composites	Hot injection <i>in situ</i> growth in m-SiO ₂ matrix	520 nm	68%	400 nm	80% after 120 h (H ₂ O)	Flexible LEDs	2019	²⁸

CsPbBr ₃ /mSiO ₂ composites	HI+ SiO ₂ coating with MPTMS	525 nm	80%	150 nm	80% after 13 h (H ₂ O)	TPA-excited PL	2020	²⁹
CsPbX ₃ @SiO ₂ nanocomposites	HI+ SiO ₂ coating with TEOS	410-680 nm	9%-84%	100 nm	60%-95% after 30 days (H ₂ O)	LEDs and cell imaging	2018	³⁰
APbX ₃ /meso-SiO ₂	<i>in situ</i> template-assisted synthesis	480-620 nm	48%-90%	Pore size 2.5-7 nm, length N/A	N/A	N/A	2016	³¹
CsPbX ₃ /meso-SiO ₂ spheres	NCs encapsulation	450-640 nm	≤55%	N/A	N/A	WLEDs	2016	³²
FAPbI ₃ @SiO ₂ composites	LARP+ TOPO	770 nm	72%	15 nm	80% after 28 days (atmosphere)	LEDs	2023	³³
CsPbI ₃ @SiO ₂ composites	HI+ SiO ₂ coating	660 - 680nm	97.5%	10.07± 0.93 nm	79% PL retention after 40 min (ethanol)	NIR LEDs	2023	³⁴
CsPbI ₃ @SiO ₂ nanocomposites	HI+ SiO ₂ coating with APTES	697 nm	N/A	13 nm	95% after 48 h (H ₂ O)	LEDs	2019	³⁵
FAPbI ₃ @TEOS	LARP+ TEOS	770 nm	57.2%	15.17 nm	80% PL retention after 7 days (Toluene/DI H ₂ O)	NIR LEDs	2023	³⁶
MAPbBr _x I _{x-3} /meso-SiO ₂	<i>in situ</i> template-assisted synthesis	500-800 nm	≤5.5%	Pore size 3.3-7.1 nm, length N/A	N/A	Solid-state LEDs	2016	³⁷

FAPbI ₃ @ APTES	LARP+ APTES	770 - 810nm	58%	16.8 nm	30% PL retention after 380 min (Toluene/DI H ₂ O)	NIR LEDs	2021	³⁸
CsPbBr ₃ @ FAPbBr ₃ @ SiO ₂ NCs	HI+ SiO ₂ coating with MPTMS	525 nm	93%	11.2 nm	90% after 240 min (H ₂ O) 81% after 240 min (isopropanol)	TPA- excited PL	2025	This work

References

- 1 I. D. Skurlov, W. Yin, A. O. Ismagilov, A. N. Tcypkin, H. Hua, H. Wang, X. Zhang, A. P. Litvin and W. Zheng, *Nanomaterials*, 2022, **12**, 1–16.
- 2 P. C. Beaumont, D. G. Johnson and B. J. Parsons, *J. Chem. Soc. Faraday Trans.*, 1993, **89**, 4185.
- 3 D. N. Dempster, T. Morrow and M. F. Quinn, *J. Photochem.*, 1973, **2**, 343–359.
- 4 R. Kapoor, C. S. Friend and A. Patra, *J. Opt. Soc. Am. B*, 2003, **20**, 1550.
- 5 M. A. Albota, C. Xu and W. W. Webb, *Appl. Opt.*, 1998, **37**, 7352.
- 6 A. Fischer, C. Cremer and E. H. K. Stelzer, *Appl. Opt.*, 1995, **34**, 1989.
- 7 W. Chen, S. Zhang, M. Zhou, T. Zhao, X. Qin, X. Liu, M. Liu and P. Duan, *J. Phys. Chem. Lett.*, 2019, **10**, 3290–3295.
- 8 A. Pramanik, S. Patibandla, Y. Gao, K. Gates and P. C. Ray, *JACS Au*, 2021, **1**, 53–65.
- 9 T. He, J. Li, X. Qiu, S. Xiao, C. Yin and X. Lin, *Adv. Opt. Mater.*, 2018, **6**, 1800843.
- 10 J. Szeremeta, M. A. Antoniak, D. Wawryńczyk, M. Nyk and M. Samoć, *Nanomaterials*, 2020, **10**, 1054.
- 11 A. Pramanik, K. Gates, Y. Gao, S. Begum and P. Chandra Ray, *J. Phys. Chem. C*, 2019, **123**, 5150–5156.
- 12 Q. Han, W. Wu, W. Liu, Q. Yang and Y. Yang, *Opt. Mater. (Amst.)*, 2018, **75**, 880–886.
- 13 K. N. Krishnakanth, S. Seth, A. Samanta and S. V. Rao, *Opt. Lett.*, 2018, **43**, 603.
- 14 W. Chen, S. Bhaumik, S. A. Veldhuis, G. Xing, Q. Xu, M. Grätzel, S. Mhaisalkar, N.

- Mathews and T. C. Sum, *Nat. Commun.*, 2017, **8**, 15198.
- 15 J. Li, Q. Jing, S. Xiao, Y. Gao, Y. Wang, W. Zhang, X. W. Sun, K. Wang and T. He, *J. Phys. Chem. Lett.*, 2020, **11**, 4817–4825.
- 16 Y. Xu, Q. Chen, C. Zhang, R. Wang, H. Wu, X. Zhang, G. Xing, W. W. Yu, X. Wang, Y. Zhang and M. Xiao, *J. Am. Chem. Soc.*, 2016, **138**, 3761–3768.
- 17 W. Song, D. Wang, J. Tian, G. Qi, M. Wu, S. Liu, T. Wang, B. Wang, Y. Yao, Z. Zou and B. Liu, *Small*, 2022, **18**, 2204763.
- 18 M. Li, X. Zhang and P. Yang, *Nanoscale*, 2021, **13**, 3860–3867.
- 19 M. Kim, J. H. Kim, M. Kim, C. S. Kim, J. W. Choi, K. Choi, J. H. Lee, J. Park, Y.-C. Kang, S.-H. Jin and M. Song, *J. Ind. Eng. Chem.*, 2020, **88**, 84–89.
- 20 T. Gu, J. Zhong, M. Ge, R. Shi, L. He and P. Bai, *J. Colloid Interface Sci.*, 2024, **657**, 580–589.
- 21 J. Park, K. Y. Jang, S. H. Lee, D.-H. Kim, S.-H. Cho and T.-W. Lee, *Chem. Mater.*, 2023, **35**, 6266–6273.
- 22 X. Feng, X. Zhang, J. Huang, R. Wu, Y. Leng and Z. Chen, *Anal. Chem.*, 2022, **94**, 5946–5952.
- 23 T. Yang, Y. Zhu, X. Yang and J. Shen, *Adv. Mater. Interfaces*, 2022, **9**, 2200571.
- 24 M. N. An, S. Park, R. Brescia, M. Lutfullin, L. Sinatra, O. M. Bakr, L. De Trizio and L. Manna, *ACS Energy Lett.*, 2021, **6**, 900–907.
- 25 X. Li, W. Cai, H. Guan, S. Zhao, S. Cao, C. Chen, M. Liu and Z. Zang, *Chem. Eng. J.*, 2021, **419**, 129551.
- 26 J. An, M. Chen, G. Liu, Y. Hu, R. Chen, Y. Lyu, S. Sharma and Y. Liu, *Anal. Bioanal. Chem.*, 2021, **413**, 1739–1747.
- 27 Q. Zhang, B. Wang, W. Zheng, L. Kong, Q. Wan, C. Zhang, Z. Li, X. Cao, M. Liu and L. Li, *Nat. Commun.*, 2020, **11**, 31.
- 28 P. Chen, Y. Liu, Z. Zhang, Y. Sun, J. Hou, G. Zhao, J. Zou, Y. Fang, J. Xu and N. Dai, *Nanoscale*, 2019, **11**, 16499–16507.
- 29 S. Li, D. Lei, W. Ren, X. Guo, S. Wu, Y. Zhu, A. L. Rogach, M. Chhowalla and A. K.-Y. Jen, *Nat. Commun.*, 2020, **11**, 1192.

- 30 N. Ding, D. Zhou, X. Sun, W. Xu, H. Xu, G. Pan, D. Li, S. Zhang, B. Dong and H. Song, *Nanotechnology*, 2018, **29**, 345703.
- 31 D. N. Dirin, L. Protesescu, D. Trummer, I. V. Kochetygov, S. Yakunin, F. Krumeich, N. P. Stadie and M. V. Kovalenko, *Nano Lett.*, 2016, **16**, 5866–5874.
- 32 H. Wang, S. Lin, A. Tang, B. P. Singh, H. Tong, C. Chen, Y. Lee, T. Tsai and R. Liu, *Angew. Chemie Int. Ed.*, 2016, **55**, 7924–7929.
- 33 W. L. Huang, W. H. Liao and S. Y. Chu, *ACS Appl. Mater. Interfaces*, 2023, **15**, 41151–41161.
- 34 Z. Pan, X. Zhu, T. Xu, Q. Xie, H. Chen, F. Xu, H. Lin, J. Wang and Y. Liu, *Appl. Sci.*, 2023, **13**, 7529.
- 35 Z. Zheng, L. Liu, F. Yi and J. Zhao, *J. Lumin.*, 2019, **216**, 116722.
- 36 W.-L. Huang and S.-Y. Chu, *Ceram. Int.*, 2023, **49**, 15802–15810.
- 37 V. Malgras, S. Tominaka, J. W. Ryan, J. Henzie, T. Takei, K. Ohara and Y. Yamauchi, *J. Am. Chem. Soc.*, 2016, **138**, 13874–13881.
- 38 L.-C. Chen, L.-W. Chao, C.-Y. Xu, C.-H. Hsu, Y.-T. Lee, Z.-M. Xu, C.-C. Lin and Z.-L. Tseng, *Biosensors*, 2021, **11**, 440.